--- Supplemental Information ---

Extraction of Dust Collected in HVAC Filters for Quantitative Filter Forensics

Alireza Mahdavi [a], Jeffrey A. Siegel [a,b]

a. Department of Civil & Mineral Engineering, University of Toronto (UofT), Toronto, Canada
b. Dalla Lana School of Public Health, University of Toronto (UofT), Toronto, Canada

Table S1: Experimental cases and extraction test conditions

Cases (1)	Filter MERV	Loading Dust	Loading Mass (g)	Sample Size	Distribution of # of Tests (2)
Phase 1: Artificial Loading (n=20)					
1	8	ISO Fine	1.2	1	1 (2)
2	8E	ISO Fine	0.8, 1.2	2	2 (1)
3	11	ISO Fine	0.6 - 13.6	7	3 (1), 2 (2), 1 (3), 1 (7)
4	14	ISO Fine	1.9	1	1 (2)
5	8	ASHRAE #2	1.8	1	1 (2)
6	8E	ASHRAE #2	1.4	1	1 (1)
7	11	ASHRAE #2	0.8 - 14.8	6	3 (1), 3 (2)
8	14	ASHRAE #2	2.0	1	1 (2)
Phase 2: Natural Loading (n=41)					
9	8	Natural	1.2 – 19.0	14	1 (1), 1 (2), 9 (3), 2 (4), 1 (6)
10	8E	Natural	1.3 - 8.6	11	1 (1), 7 (3), 2 (4), 1 (6)
11	11	Natural	2.4 - 12.7	6	3 (3), 2 (4), 1 (6)
12	14	Natural	1.1 – 16.7	10	7 (3), 2 (4), 1 (6)

(1) Cases # 3 and #7 are the base cases in Phase 1 (bolded and underlined).
(2) # in parentheses are the number of extraction cycles associated with each # of the tests.

Filters Selected

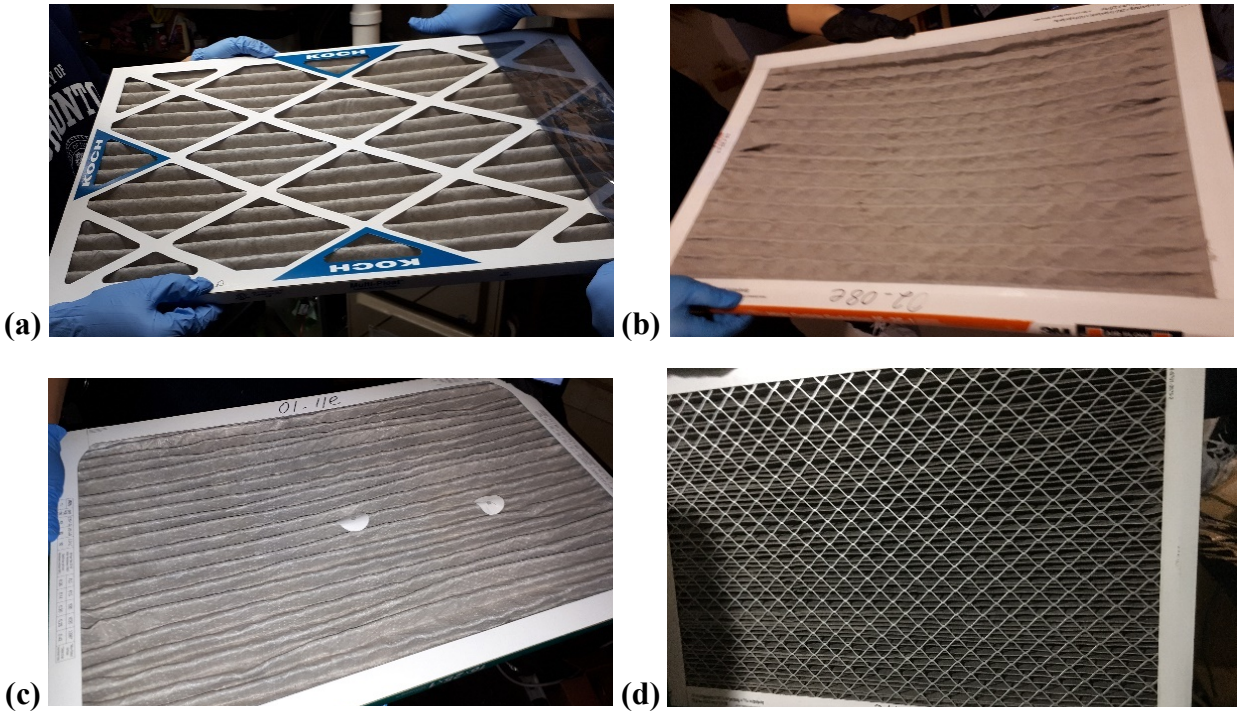

Figure S1: a) MERV 8, b) MERV 8E, c) MERV 11, and d) MERV 14 filters. Size of all the filters used in Phase 1 was 41 × 64 cm × 2.5 cm. Sizes of filters varied in Phase 2 depending on the recruited homes HVAC size

Test Dust Samples

We measured the size distribution data presented in Figure S2 and Table S2 using a laser diffraction particle sizer (LDPS) (Malvern, Mastersizer 3000). We input the average density and refractive index (RI) of 2.8 (g/cm^3) and 1.6 (-), respectively, into the LDPS calculated by the following formulas:

$$\rho_{ave} = \frac{1}{\sum_{i=1}^{N} \frac{m_i}{\rho_i}} \qquad RI_{ave} = \sum_{i=1}^{N} \frac{\frac{m_i}{\rho_i}}{\sum_{i=1}^{N} \frac{m_i}{\rho_i}} \times RI_i$$

m_i, ρ_i, and RI_i are the mass fractions, densities, and the RIs of the components of the Arizona test dust (ATD) identified in the ISO Fine test dust sample given in Table S3. The subscript i refers to the components and N refers to the total number of components.

Due to the likely similarity of milled cotton linters RI to 1.6 (-) (the average calculated RI of ISO Fine), we did not change the average RI of ASHRAE#2 (Malvern, 1997). We did not either change the average density of the ASHRAE #2 test dust since the cotton linters were 6.5% of the total dust and also, we found the density would not impact the volumetric distribution results. We also selected the absorption index (AI) default value of 0.1 as this resulted in the best fit

between the measured and published cumulative size distributions of the ISO Fine test dust using the calculated densities and RIs (see Figure S2).

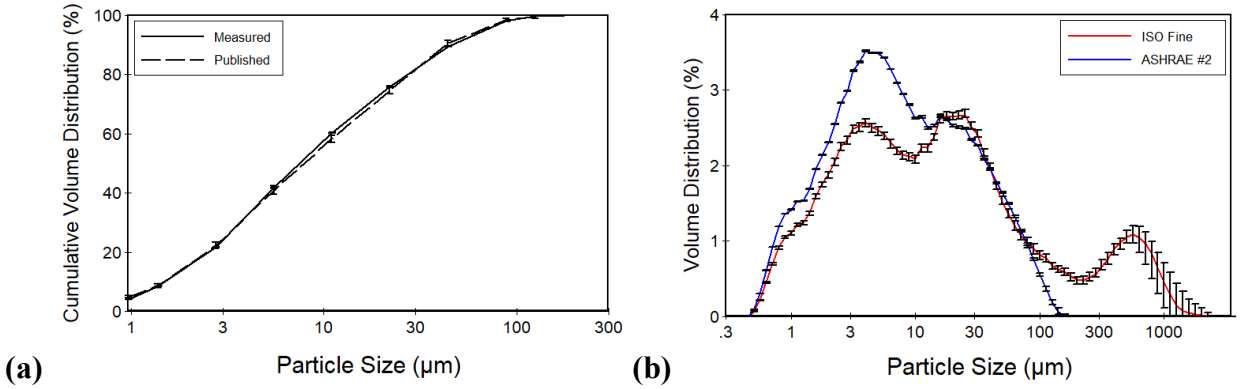

Figure S2: a) Measured and published cumulative size distribution of the ISO Fine test dust samples. b) Particle size distribution of ISO Fine and ASHRAE#2 test dust samples.

Table S2: Test dust information

Test Dust	Particle Size Distribution (µm) (1,2)					Composition
	D-0	D-10	D-50	D-90	D-100	
ISO Fine	0.45 (1.0)	1.5 (1.0)	7.3 (1.0)	45.3 (1.0)	166 (1.1)	Arizona Test Dust (ATD)
ASHRAE#2	0.45 (1.0)	1.8 (1.0)	13.7 (1.0)	308 (1.3)	1546 (1.3)	ATD (93.5%) + milled cotton linters (6.5%)

(1) x in D-x is the particle size (in µm) under which x% of the size distribution lies. D-0 and D-100 represent the upper and lower particle size range.
(2) Numbers are geometric mean (GM) from the five runs of the same sample. The numbers in parentheses are the geometric standard deviation (GSD) from the five runs of the same sample.

Table S3: ATD composition and component properties

Component	Mass Fraction (%) (1)	RI (-) (2)	Density (g/cm^3) (3)
SiO_2	68-78	1.48	2.65
Al_2O_3	10-15	1.765	3.95
Fe_2O_3	2-5	3.01	5.24
Na_2O_3	2-4	n.a.	2.27
CaO	2-5	1.838	3.35
MgO	1-2	1.735	3.58
TiO_2	0.5-1	2.605	4.23
K_2O	2-5	n.a.	2.35

(1) ATD material safety data sheet (MSDS)
(2) Malvern (1997) "Sample Dispersion and Refractive Index Guide"
(3) Haynes (2012) "CRC Handbook of Chemistry and Physics"

Filter Loading

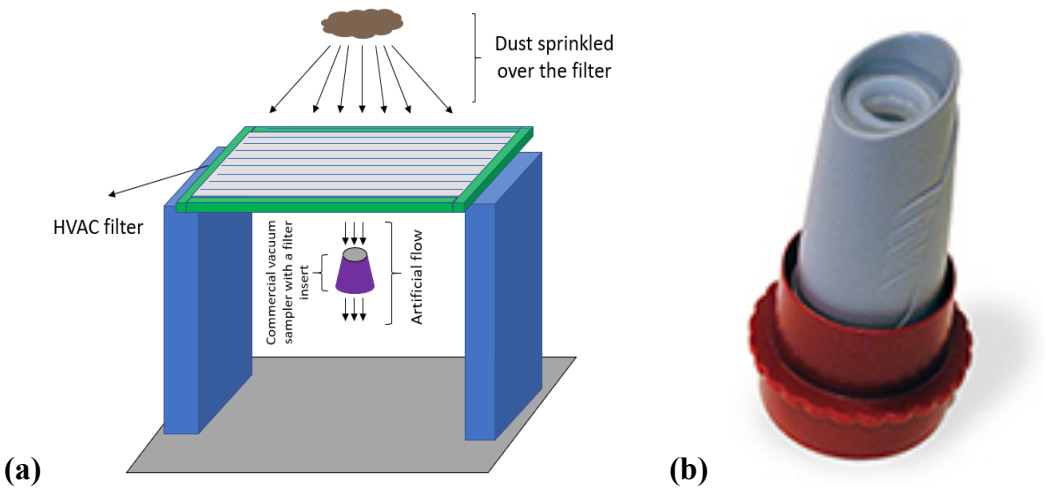

Figure S3: a) Filter holder for artificial loading, b) Commercial sampler

Based on our best possible estimate, we tried to identify the size distribution of the dust loaded in the filter using Eq. (S1):

$$\left(\frac{dV}{V}\right)_d = \frac{M_{tot}\ \left(\frac{dV}{V}\right)_{tot} - \left(M_{backflow}\right)\left(\frac{dV}{V}\right)_{backflow}}{M_{tot} - M_{backflow}} \qquad \text{(S1)}$$

The terms dV/V and M in Eq. (S1) represents the size distribution and masses and the subscripts "tot", "d", and "backflow" represent the dust sprinkled, captured by filter, and stuck in the backflow filter high-efficiency particulate air (HEPA) filter insert. Figure S4 illustrates the size distribution of the dust loaded in filter calculated from the above equation as well as the test dust sample sprinkled over the filter for one of the scenarios where the dust mass passing through the filter was greatest compared to the dust captured in the filter (44%). With acknowledging the limitations of this procedure (e.g., lack of control on any dust mass that can be resuspended into the ambient air), the maximum cumulative difference between the volume distribution captured on the filter and the original test dust was no more than 6% (with a mean of 1.5% across all the size channels).

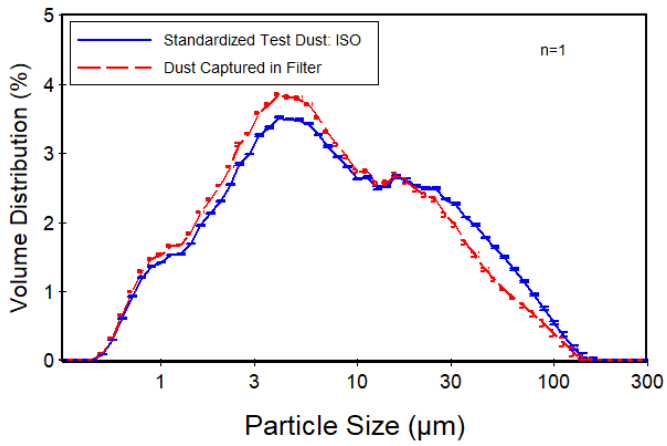

Figure S4: Comparison between the size distributions of the test dust and dust captured in the filter for a case of MERV 8E filters loaded with ISO

Extraction Vacuum Sampler

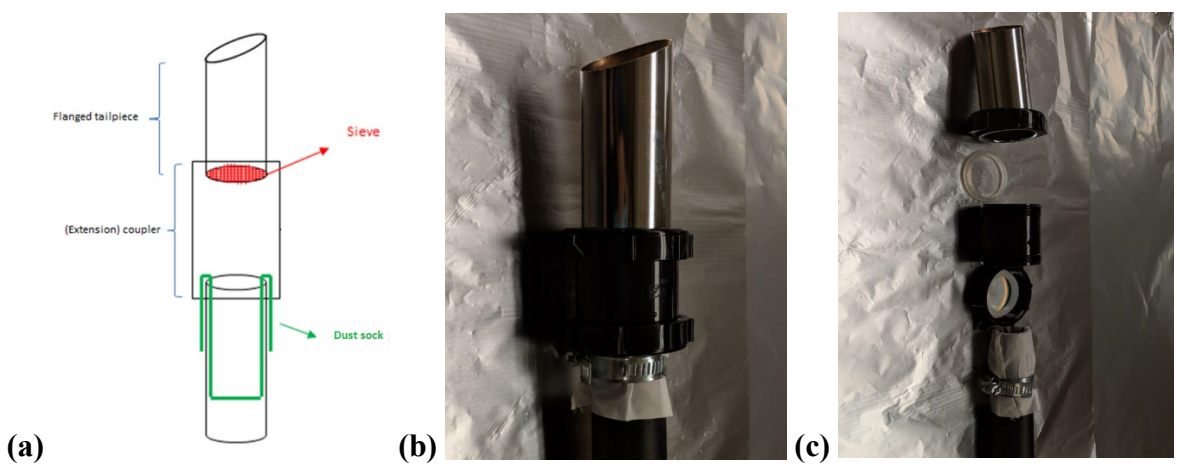

Figure S5: The high-suction vacuum sampler: a) schematic, b) assembled, and c) disassembled

Dust Accessory Cleaning

To ensure no contamination, we always used a clean sampler set for the extraction from each separate filter. In Phase 1, to clean all the sampler parts except the dust socks, we:

1- Washed the items with water and soap;
2- Rinsed the items with tap or distilled water; and
3- Dried and wiped the item with isopropanol (IPA).

The dust socks and the Petri dishes were used as received (deemed clean). The cleaning procedure in Phase 2 was more complex due to the importance of samples recovered for future filter forensics analyses and a need to minimize contamination. To clean all the metallic parts (e.g., flanged tailpiece, sieves, clamps, tweezers, and spatulas), we:

1- Washed the item by water and soap to remove any dust, dirt or visible contamination;
2- Soaked the item in a 10% v/v Decon solution for at least 1-2 hours;
3- Rinsed the item with high-pressure liquid chromatography (HPLC)-grade water;
4- Dried the item in an oven at ~100 ^{0}C for about 1-2 hours;
5- Disinfected the item by rinsing it with Acetone, Dichloromethane, and n-Hexane.

To clean the plastic, polymer, and PVC parts (e.g., coupler, rings, wand, and plastic funnels), we followed everything mentioned above except the last two stages. Instead, we dried the items and wiped them using IPA.

The amber glass vials carrying the dust were cleaned after we:

1- Washed the item by water and soap to remove any dust, dirt or visible contamination on or inside the vial;
2- Soaked the item in a 10% v/v Decon solution overnight (at least 12-16 hours);
3- Rinsed the item using HPLC grade water; and
4- Baked the vials in an oven at ~ 235 °C overnight (at least 12-16 hours).

To clean the caps of the vials, we soaked them inside a 10% v/v Decon solution for about 20 minutes while we sonicated the solution. Then, we sonicated them in HPLC grade water for 10 minutes to initially remove the Decon. We finally rinsed all the caps using HPLC grade water to ensure no Decon is left on the caps. To clean the dust socks, we inserted the socks in the accelerated solver extractor Dionex ASE 350 using filter grade hexane at 90 °C and 1500 psi for a 5-minute heat time, 5-minute static time, 100% flush volume, 30-s purge time, and 8 static cycles. The dust socks were fully covered and stored in pre-cleaned aluminum foils baked under 450 °C and kept in the freezer at -20 °C.

Homogeneity Tests

To ensure that adding the recovered dust from multiple extraction cycles of the same filter does not majorly change the particle size distribution of a cumulatively recovered sample, we measured the size distribution of the dust recovered from the most heavily loaded filter among the Case #3 filters (see Table S1) twice. We first took a small fraction of the dust recovered after the first cycle and added it to the LDPS. We then continued the extraction for another six cycles (7 cycles total) and added the recovered dust to the sample left from the first cycle. After all the 7 cycles, we added the cumulative sample recovered to the LDPS and measured the size distribution again. Figure S6 illustrates the data obtained from this procedure and indicates minor deviation from the two curves particularly between 0.3-60 µm ($p>0.05$, Kolmogorov-Smirnov).

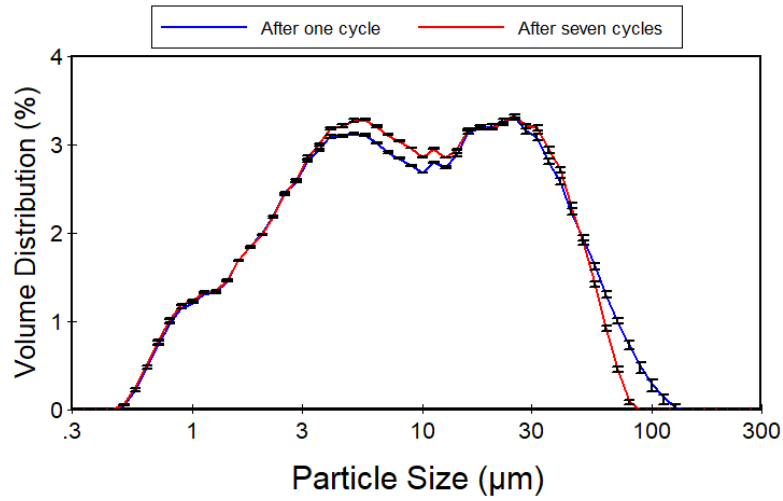

Figure S6: Particle size distribution of dust samples recovered after one and seven extraction cycles from a heavily-loaded MERV 11 filter. Error bars represent the minimum and maximum volume distribution among the five runs of the same sample.

Extraction Processes: Dust Gain and Loss

To explore more about our extraction technique and understand dust gain (and loss) mechanisms, we defined three efficiency terms based on the three major processes that occurred during the recovery of dust by the after-sieve portion of the sampler, since this fraction was generally more useful for filter forensics due to the removal of larger flocs and particles. These processes were:

1- Suction: Resuspension/detachment of dust from the filter by suction airflow applied by the vacuum sampler,
2- After-sieve collection: Collection of dust by the after-sieve parts which were dust sock and the inner wall of the coupler.
3- Transfer: transfer of dust from the dust sock and the inner wall of the coupler into the storage container.

Eqs. (S2) to (S4) express the three efficiency terms corresponding to the processes introduced above in any extraction cycle. The after-sieve recovery efficiency, which is the product of the three mentioned processes efficiencies, is presented in Eq. (S5). Eq. (S6) expresses the pre-sieve recovery efficiency.

$$\eta_{su,i}(\%) = \frac{M_{v,i}}{M_d} = \frac{M_{i-1} - M_i}{M_0 - M_{bl}} \quad \text{(S2)}$$

$$\eta_{asc,i}(\%) = \frac{M_{fsc,i}}{M_{v,i}} = \frac{M_{fsc_full_i} - M_{fsc_clean,i}}{M_{i-1} - M_i} \quad \text{(S3)}$$

$$\eta_{t,i}(\%) = \frac{M_{as,i}}{M_{fsc,i}} = \frac{M_{cas,i} - M_{cas,i-1}}{M_{fsc_full_i} - M_{fsc_clean,i}} \quad \text{(S4)}$$

$$\eta_{as,i}(\%) = \eta_{su,i} \times \eta_{asc,i} \times \eta_{t,i} = \frac{M_{as,i}}{M_d} = \frac{M_{cas,i} - M_{cas,i-1}}{M_0 - M_{bl}} \quad \text{(S5)}$$

$$\eta_{s,i}(\%) = \frac{M_{s,i}}{M_d} = \frac{M_{cs,i} - M_{cs,i-1}}{M_0 - M_{bl}} \quad \text{(S6)}$$

η_{su}, η_{asc}, and η_t refer to the suction, after-sieve collection, and transfer efficiencies, respectively. Figure S7 illustrates the concept of these processes and their efficiency terms.

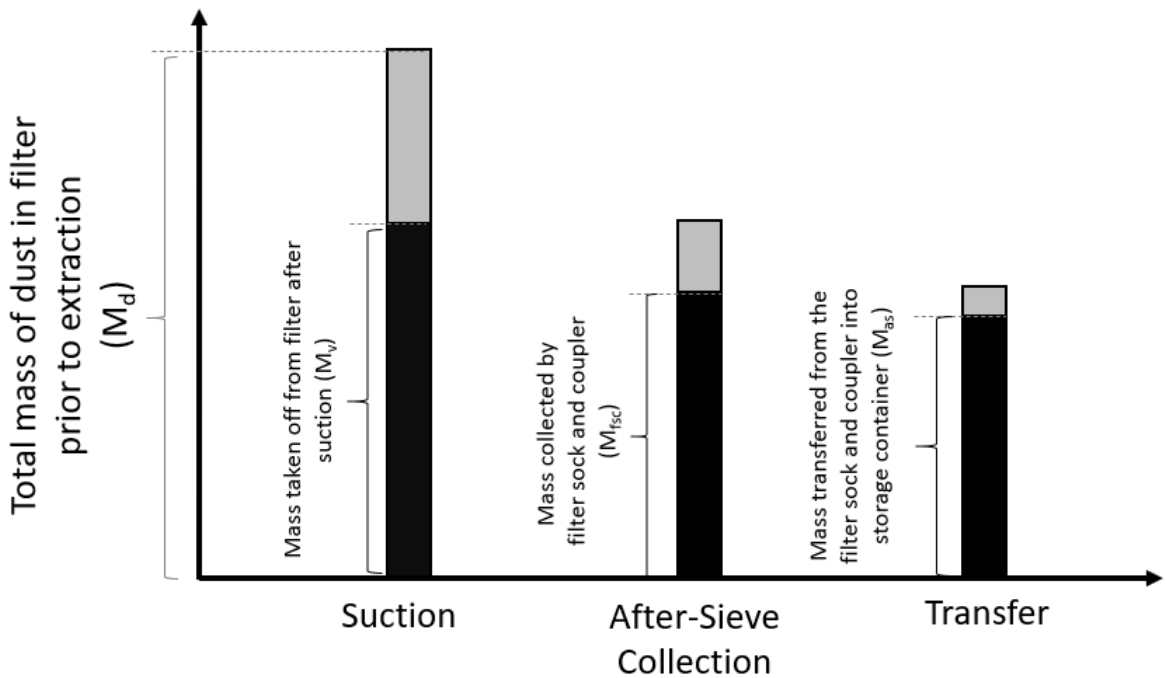

Figure S7: The visual concept of the suction, after-sieve collection, and transfer efficiencies.

To identify any amount of the loss of dust during the extraction, we defined the extraction mass closure (MC_E), the ratio of overall dust recovery to the total mass suctioned from the filter (M_v) described in Eq. (S7).

$$MC_{E,i}(\%) = \frac{M_{as,i} + M_{s,i}}{M_{v,i}} = \frac{(M_{cas,i} - M_{cas,i-1}) + (M_{cs,i} - M_{cs,i-1})}{M_{i-1} - M_i} \quad \text{(S7)}$$

Ideally, a unity MC_E (i.e., 100%) corresponds to a complete overall recovery of all the dust suctioned from the filters by the after-sieve or pre-sieve parts. A smaller MC_E highlights any loss of dust mass during the extraction process due to resuspension and dispersion into the ambient without being captured by the pre- or after-sieve parts of the sampler or particles that penetrated the dust sock.

The subscript 'i' in the Eqs. (S2) to (S7) refers to the extraction cycle number (i: 1 → n (n ϵ N), e.g., i=1: first cycle, i=2: second cycle). n is the total number of extraction cycles done over a filter. Using the above equations, we calculated cumulative suction, pre- and after-sieve recovery efficiencies, and the extraction mass closure performed over n cycles re-written in Eqs. (S8) to (S11). Table S4 summarizes all the symbols used in Eqs. (S2) to (S11).

$$\eta_{su,cum}(\%) = \sum_{i=1}^{n} \eta_{su,i} = \sum_{i=1}^{n} \frac{M_{i-1} - M_i}{M_0 - M_{bl}} = \frac{M_0 - M_n}{M_0 - M_{bl}} \quad \text{(S8)}$$

$$\eta_{as,cum}(\%) = \sum_{i=1}^{n} \eta_{as,i} = \sum_{i=i}^{n} \frac{M_{cas,i} - M_{cas,i-1}}{M_0 - M_{bl}} = \frac{M_{cas,n} - M_{cas,0}}{M_0 - M_{bl}} \quad \text{(S9)}$$

$$\eta_{s,cum}(\%) = \sum_{i=1}^{n} \eta_{s,i} = \sum_{i=i}^{n} \frac{M_{cs,i} - M_{cs,i-1}}{M_0 - M_{bl}} = \frac{M_{cs,n} - M_{cs,0}}{M_0 - M_{bl}} \quad \text{(S10)}$$

$$MC_{E,cum}(\%) = \sum_{i=i}^{n} \frac{M_{as,i} + M_{s,i}}{M_{v,i}} = \frac{\sum_{i=1}^{n}[(M_{cas,i} - M_{cas,i-1}) + (M_{cs,i} - M_{cs,i-1})]}{\sum_{i=1}^{n}(M_{i-1} - M_i)} = \frac{(M_{cas,n} - M_{cas,o}) + (M_{cs,n} - M_{cs,o})}{(M_0 - M_n)} \quad \text{(S11)}$$

Table S4: Mass terms measured during the extraction procedure

Terms	Definition	Measurement [1]
M_{bl}	Mass of blank (i.e., unloaded) filter	Balance
M_0	Mass of loaded filter after it is taken down (before extraction)	Balance
M_d	Mass of dust loaded in the filter (constant)	M_0 - M_{bl}
M_i	Mass of loaded filter after the 'i'th extraction cycle	Balance
$M_{v,i}$	Mass of dust suctioned from the filter after the `i'th extraction cycle.	$M_{i-1} - M_i$
$M_{fsc_clean,i}$	Mass of empty dust sock (and clean coupler) before the 'i'th extraction	Microbalance
$M_{fsc_full,i}$	Mass of full dust sock (of dust) and the coupler after the 'i'th extraction	Microbalance
$M_{fsc,i}$	Mass of dust captured by the dust sock and coupler after the `i'th extraction cycle	$M_{fsc_full,i} - M_{fsc_clean,i}$
$M_{cas,0}$	Mass of empty container (without any dust collected) that will hold the after-sieve dust (nominal < 1mm).	Microbalance
$M_{cas,i}$ [2]	Mass of the container holding the after-sieve dust (cumulatively added) [4] after 'i' cycle(s) of extraction.	Microbalance
$M_{cs,0}$	Mass of empty container (without any dust collected) that will hold the pre-sieve dust (nominal > 1mm).	Microbalance
$M_{cs,i}$ [3]	Mass of the container holding the pre-sieve dust (cumulatively added) [5] after 'i' cycle(s) of extraction.	Microbalance
$M_{as,i}$	Mass of dust recovered from the after-sieve parts after the `i'th extraction cycles	$M_{cas,i}$ - $M_{cas,i-1}$
$M_{s,i}$	Mass of dust recovered from the sieve after the `i'th extraction cycles	$M_{cs,i}$ - $M_{cs,i-1}$

(1) Balance and microbalance refer to Sartorius MSE3203S and MSE225S, respectively.
(2) The same container was often used to cumulatively collect the after-sieve dust from all extraction cycles of the same filter.
(3) The same container was often used to cumulatively collect the sieve dust (nominally >1000 μm) from all extraction cycles of the same filter.

Figure S8 illustrates the efficiencies corresponding to the three processes taking place during the extraction: suction, after-sieve collection, and transfer (described in Eqs. (S2)-(S4)) as well as the individual after-sieve recovery efficiency, the product of the three mentioned efficiency terms in both phases. Suction was consistently the least efficient process among the three processes ($p<0.01$, signed-rank test) with an efficiency ranged from 1.2 – 56.0% (median= 24.7%) in Phase 1 and 0.6 – 79.4% (median = 13.0%) in Phase 2. Low suction efficiencies highlight that a substantial dust amount is left unvacuumed inside the filter after extraction. In Phase 1, the non-cumulative suction (and recovery) efficiency were significantly lower during the second cycle compared to the first cycle ($p<0.01$, rank-sum test). After that the filter was vacuumed during the first cycle, the remaining dust in the filter was embedded in the deeper layers of filter media. The

extraction of dust embedded in the deeper layers of filter media could be more difficult due to stronger binding forces between the particles and filter fibers to which particles were attached, particularly when the loading is moderate or low (such as in Phase 1). Collection by the after-sieve parts (i.e., dust sock and coupler) ranged over 13.8 – 98.9% (median = 71.6%) in Phase 1 and 2.2 – 86.1% (median = 34.8%) in Phase 2. Lack of a 100% after-sieve collection efficiency indicates that out of all the dust particles removed from the filter due to suction, some are dispersed into the ambient air, some are captured by the sieve, and/or some are lost by passing through the dust sock. The after-sieve collection efficiency was on average less in Phase 2 due to more dust captured by the sieve. Transfer from the after-sieve parts into the Petri dishes was the most efficient process with an efficiency ranging from 39.9 – 99.2% (median=83.4%) in Phase 1 and 55.9 – >100% (median 91.8%) in Phase 2 indicating minimal loss of dust during its transfer from the dust sock and coupler into the containers ($p<0.01$, signed-rank test: comparison of transfer vs. suction or transfer vs. after-sieve collection). The transfer efficiency of >100% is evidence of recovered dust from previous cycles left inside the dust sock being mixed with newly recovered dust in a later cycle transferred into the storage containers.

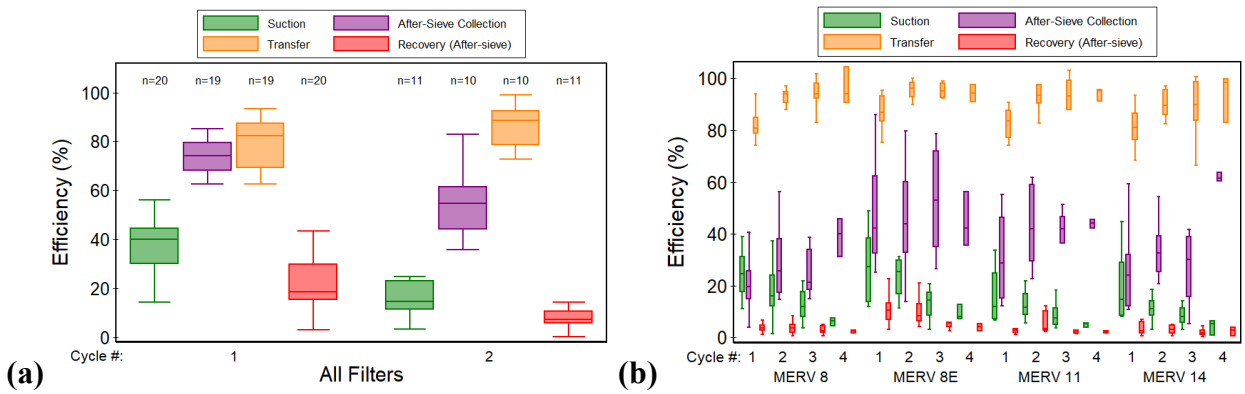

Figure S8: Efficiency terms of suction (non-cumulative), after-sieve collection, and transfer processes as well as recovery (non-cumulative) in terms of extraction cycle number: a) artificially loaded filters, b) naturally loaded filters.

Figures S9a and S9b illustrate the extraction mass closure (MC_E), the ratio of the overall mass of dust recovered from the filter to the total mass of dust suctioned from the filter, from the two phases (cumulatively measured). With most of our cases, we experienced a mass closure much less than 100% highlighting the loss of dust during extraction. Also, the extent of loss varied within or between phases or filters: 29.0 – 81.4% (median =58.9%) in Phase 1 and 2.3 – 86.9% (median = 50.6%), 25.8 – 95.0% (median = 72.5%), 14.2 – 95.4% (median = 51.7%), and 9.6 – 80.4% (median = 29.8%) for MERV 8, 8E, 11, and 14 filters, respectively, in Phase 2, after the first extraction cycle.

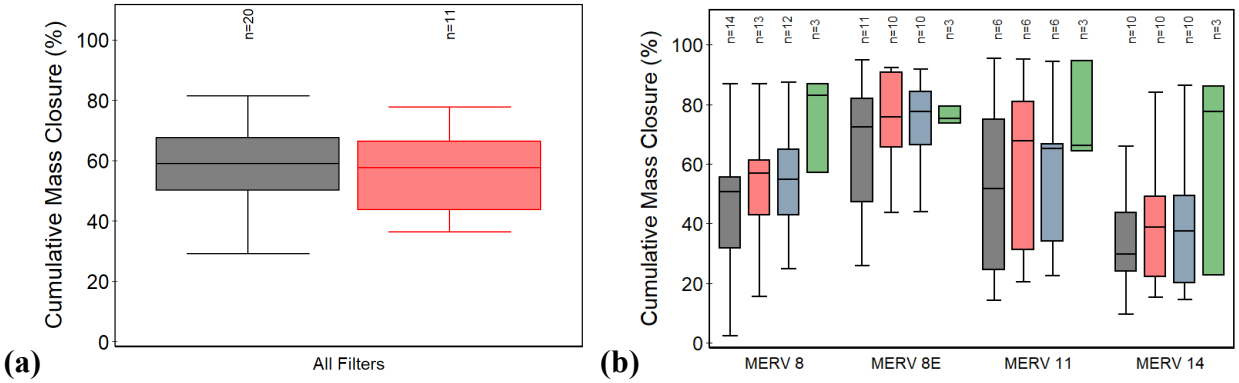

Figure S9: Cumulative mass closure in terms of filter type and cycle number. a) Phase 1: artificial loading, b) Phase 2: natural loading. Colors denote cycle numbers (black: 1, red: 2, blue: 3, and green: 4)

Other Recovery and Representativeness Results

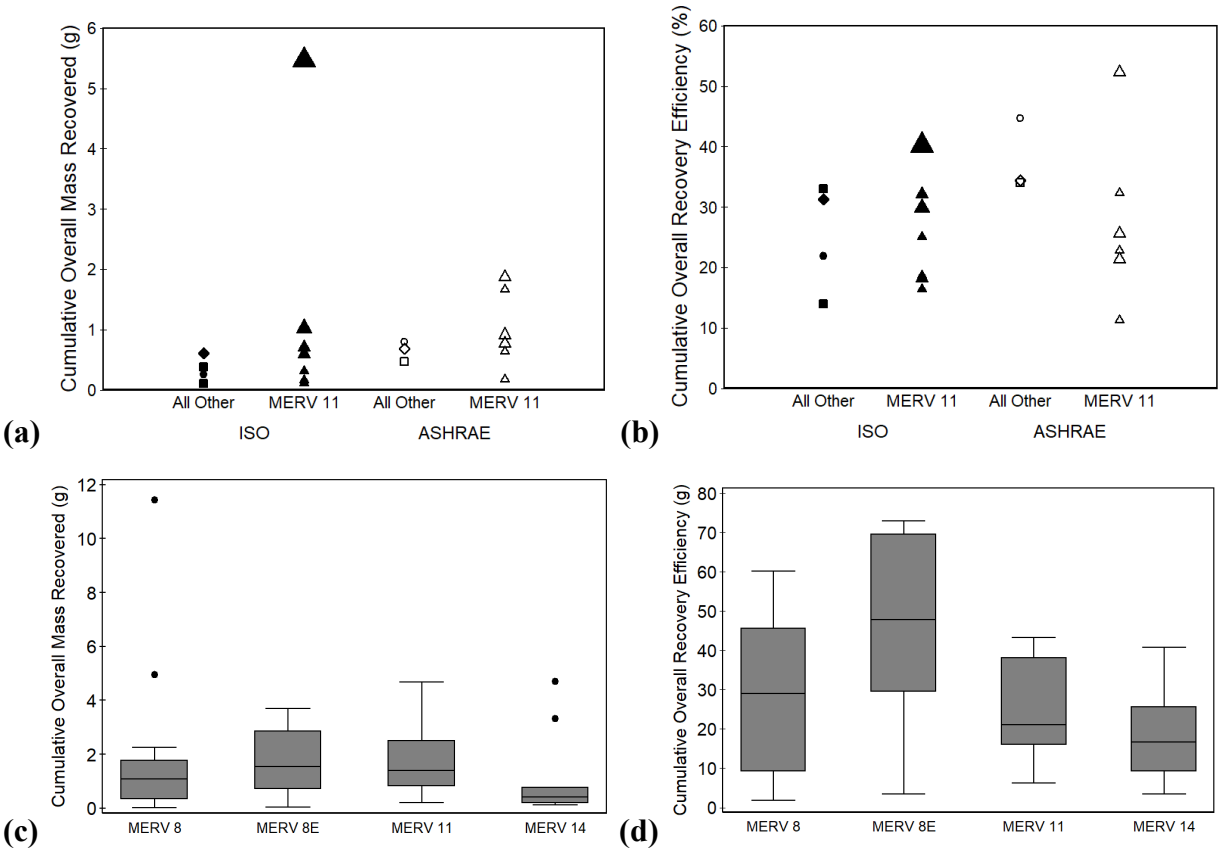

Figure S10: The cumulative overall mass recovered and recovery efficiency after the maximum number of extraction cycles: a, b) artificially loaded filters (Phase 1), c, d) naturally loaded filters (Phase 2). Markers sizes in (a) and (b) correlate to the number of cycles performed over the filter.

Multiple extractions on a heavily loaded filter: In Figure S11, we recovered a cumulative 5.5 g of dust from a MERV 11 filter (equivalent to 40.2% recovery efficiency) after doing 7 extraction cycles. This suggests that, for very heavily loaded filters, the later extraction cycles can be sometimes as effective as or even more effective than the earlier cycles. So, continuing the extraction of heavily loaded filters with more cycles will be still beneficial for dust recovery, and the amount of recovery in later cycles does not necessarily diminish if plenty of dust is loaded in the filter.

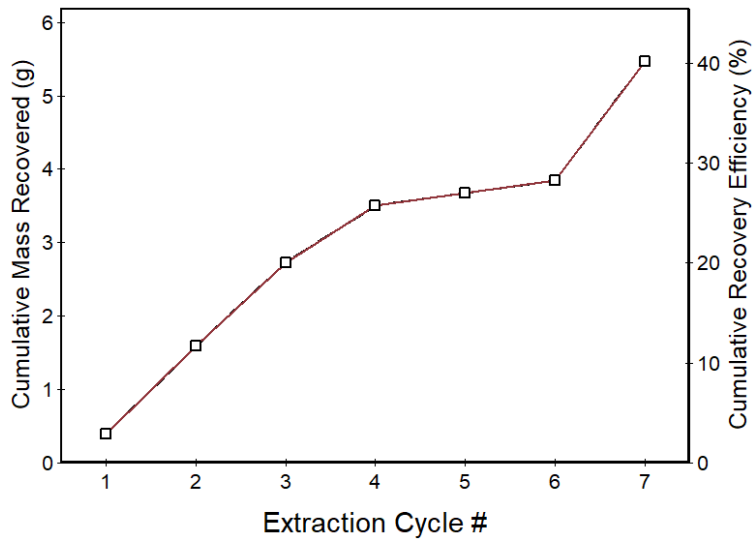

Figure S11: The cumulative mass recovery (left axis) and recovery efficiency (right axis) after seven cycles of extraction from a MERV 11 filter loaded with 13.6 g of ISO.

Correlation of dust recovery and loaded mass: The influence of loaded mass on the recovery of dust was mixed and complex. We sometimes found a strong correlation between the cumulative mass recovered and the mass loaded in the filter using Spearman's rank correlation coefficient test even after excluding the two observations with a high dust mass loaded in the filter (~14 g) (ρ: 0.77 – 0.92, $p < 0.001$) (Figure S12a,c). The correlation between the two parameters was still strong for the filters going through at least two extraction cycles (ρ: 0.7 – 0.72, $p < 0.02$) (Figure S12b and S12d). However, after excluding the heavily loaded filter from the cases where we performed at least two extraction cycles, no correlation was observed (ρ: 0.62, $p > 0.05$) that may suggest a weak influence of the loaded mass on the recovery amount over lightly loaded filters (Figures S12b and S12d).

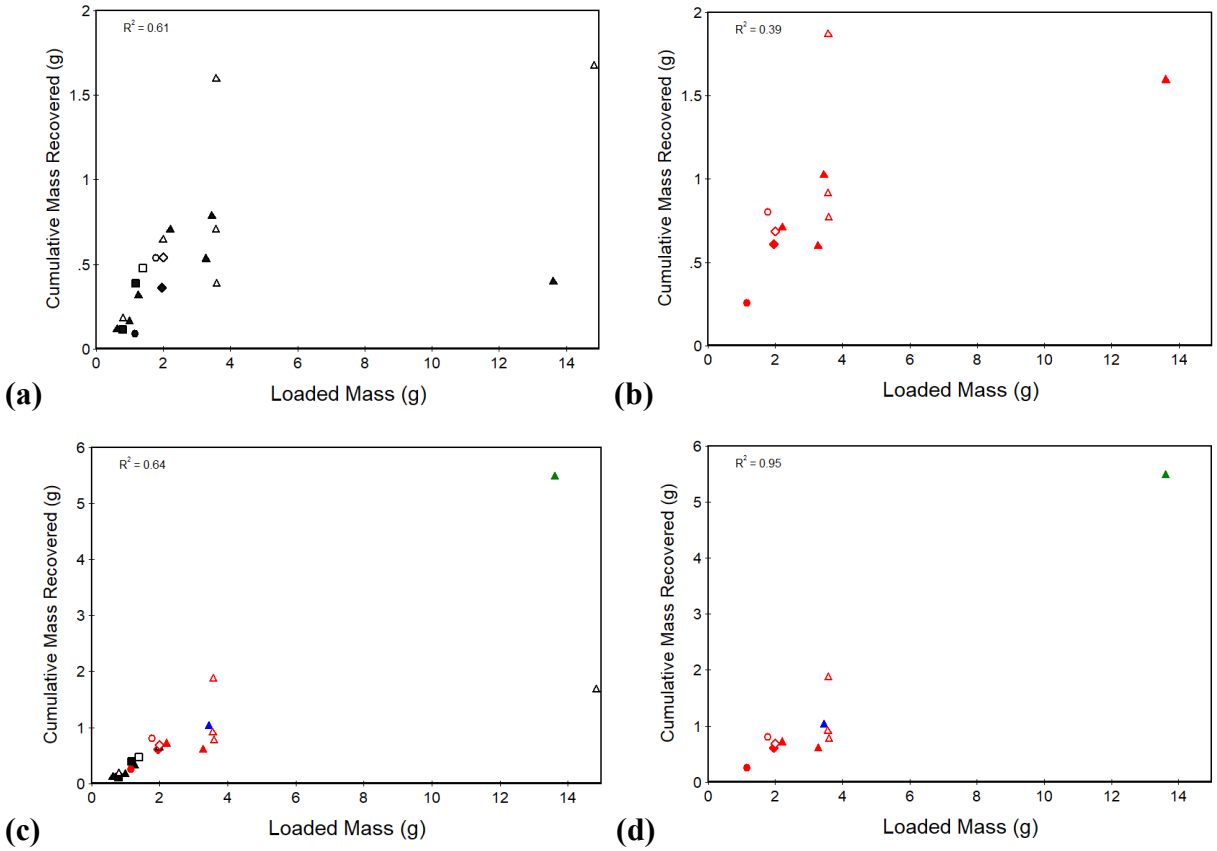

Figure S12: Mass of the dust recovered from the artificially loaded filters (Phase 1): a) after a single extraction cycle (n=20), b) after two extraction cycles (n=11), c) after the maximum number of cycles applied (varying from 1 to 7) (n=20), and d) after the maximum number of cycles applied for the filters that experienced at least two extraction cycles (n=11). Markers shapes denote filter type (circle: MERV 8, square: MERV 8E, triangle: MERV 11, and diamond: MERV 14). Fill status denotes the test dust with which filters were loaded (filled: ISO, hollow: ASHRAE). Colors denote different cycle numbers (black: cycle 1, red: cycle 2, blue: cycle 3, and 4: cycle number greater than 3)

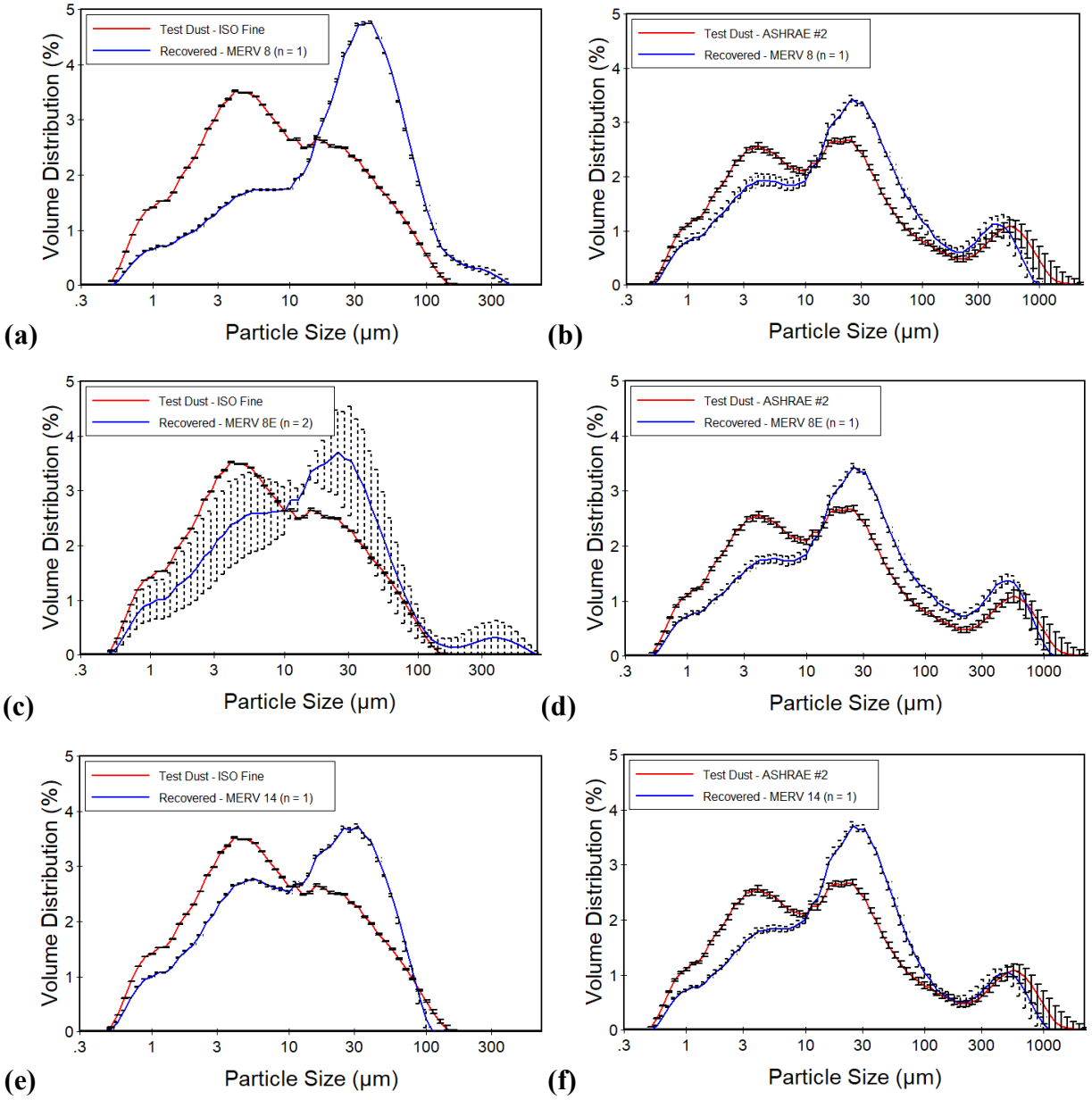

Figure S13: Particle size distribution of ISO and ASHRAE test dust and the recovered dust from MERVs 8, 8E, and 14 filters (i.e., non-base cases). n refers to the number of analyzed samples.

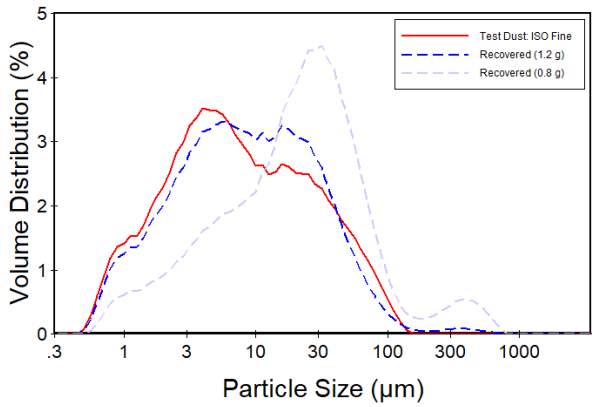

(a)

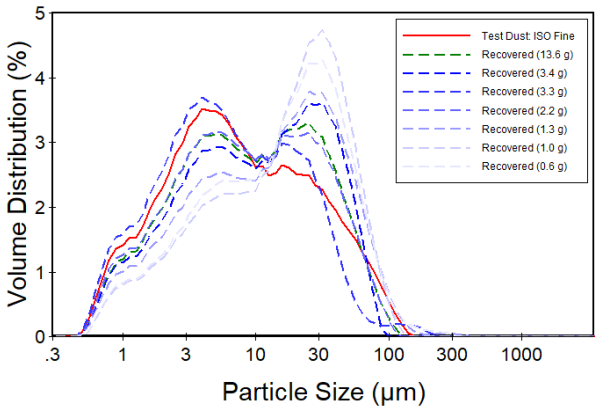

(b)

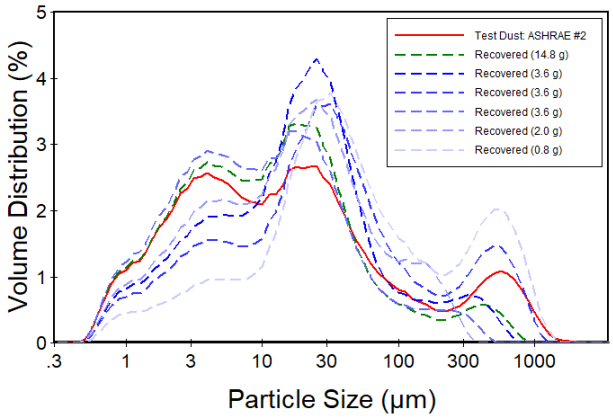

(c)

Figure S14: Particle size distribution of the recovered dust from individual experiments, a) MERV 8E loaded with ISO, b) MERV 11 loaded ISO, and c) MERV 11 loaded with ASHRAE. Values in parentheses inside the legend represent the amount of dust loaded in the filters. Green dashed lines represent extraction from the heavily loaded filters (loading mass ~ 14 g)

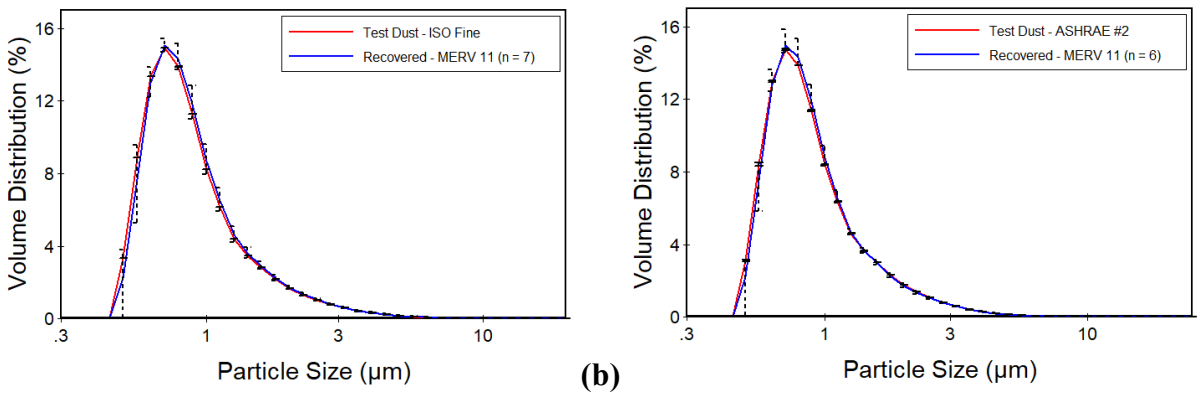

Figure S15: Count-based particle size distributions of test and recovered dust samples (a) ISO-loaded and (b) ASHRAE-loaded cases. Error bars on the size distribution of the recovered samples represent the minimum and maximum count channel distributions from all runs of all replicates.

Influence of sieve and the representativeness of the overall recovered dust: Figure S16a illustrates the size distributions of the test dust as well as the pre- and after-sieve dust recovered from all the filters for which we measured the size distribution of both fractions (n=5) to discover any influence of the sieve on the sample representativeness. Error bars represent the minimum and maximum volume fractions among five runs of the same sample for test dust and otherwise minimum and maximum volume fractions among all runs of all samples. These five filters were all loaded with ASHRAE test dust. On average, there was reasonably similarity between the test and pre-sieve dust curves, but there was also a much higher variation in the volume fractions of all size channels of the pre-sieve curve when compared to the after-sieve curve (Figure S16a). One of the reasons for these high variations was the existence of larger particles in the pre-sieve samples. Due to their size/weight, these particles could not always stay suspended in the water so the LDPS could not detect them in all but some of the runs resulting in such big variations in their distributions. Given the distributions were normalized (i.e., the sum of the distributions from all the channels was 100%), these big variations also influenced the distribution of smaller particles causing large variations throughout the size distribution curves. These findings support that the sieve is useful to make the dispersed sample free from larger particles, reduce the variations across the whole size distribution span, and lead to more repeatability of the LDPS results.

In one of these five cases, we also combined the pre- and after-sieve dust samples and measured the size distribution of combined dust (labeled as "recovered – combined") along with the size distribution of the test, pre-sieve, and after-sieve dust (Figure S16b). The combined dust would be a representative of the overall recovered dust if we did not use a sieve in our sampler. After analyzing all the test, pre-sieve, after-sieve, and combined dust, we observed that the size distribution of the pre-sieve dust was more proximate to that of the test dust. This proximity might suggest that a sieve can sometimes capture a more representative sample of the dust loaded in the filter. However, the size distribution of the combined dust (pre-sieve + after-sieve) was more proximate to that of the after-sieve dust as both samples underrepresented particles <

10 µm. The latter proximity suggests the use of the sieve cannot majorly influence the representativeness of the recovered sample. The fact that the size distributions of the after-sieve and combined dust samples are closer to each other, despite the more proximity of the size distributions between the test and pre-sieve recovered samples, is because there has been much less amount of mass recovered by the sieve compared to what recovered by the after-sieve parts (0.1 g vs. 0.7 g in this specific case) so the size distribution of the combined dust is dominated by the after-sieve dust. Overall, we found there is no major reason not to use the sieve during the extraction of dust using vacuum samplers because, first, it does not majorly influence the representativeness of the after-sieve dust and, second, it helps to stabilize a dispersed sample by reducing variations and uncertainties across the entire size distribution domain by filtering its large particles.

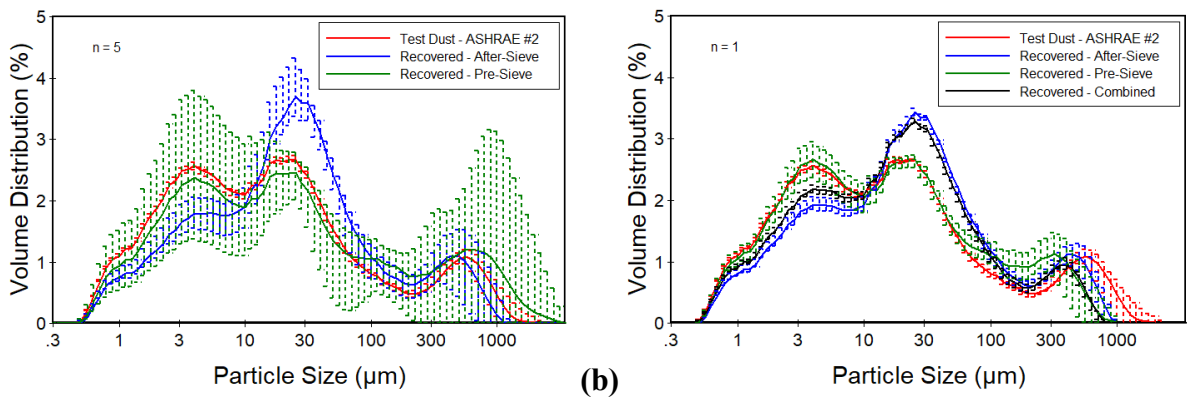

Figure S16: Influence of sieve on the particle size distribution of the dust recovered from the artificially loaded filters and sample representativeness

Modal analysis: The following log-normal particle size distribution formula was used for curve-fitting of the test dust overall size distributions (Seinfeld and Pandis 2016):

$$\frac{dV}{d\ \ln D_p} = \frac{V}{(2\pi)^{(\frac{1}{2})} \ln \sigma_g} \exp\left(-\frac{(\ln D_p - \ln \overline{D_{pg}})^2}{2\,(\ln \sigma_g)^2}\right) \tag{S12}$$

$\frac{dV}{d\ \ln D_p}$ and D_p in Eq. (S12) are the size distribution (i.e., function) and particle size (i.e., variable), respectively. $\overline{D_p}$ and σ_g are the geometric mean (GM) and geometric standard deviation (GSD) of the lognormal distribution, respectively. The ISO and ASHRAE test dust samples were fitted with three and six log-normal distribution modes, respectively. In Table S5, we summarized the geometric mean (GM), geometric standard deviation (GSD), and volume fraction of all these modes constituting the overall size distributions of the two test dust samples. Given the ASHRAE was a mixture of ISO and cotton linters (ASHRAE 2017), the first three modes of ASHRAE test dust had the same GMs and GSDs as those in ISO. The other three modes in the ASHRAE were identified using the location of the other peaks in the size distribution of ASHRAE test dust. Figure S17 shows the modal analysis for the test dust samples.

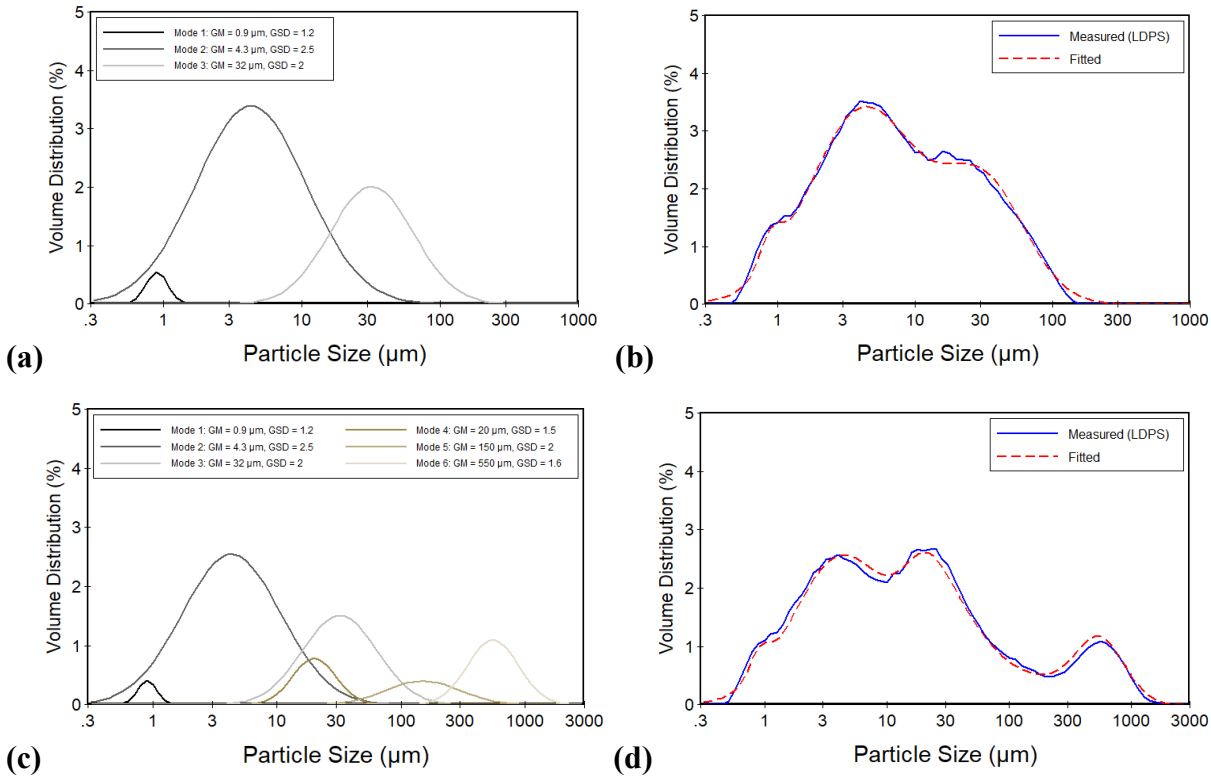

Figure S17: a, c) Individual modes constituting ISO and ASHRAE test dust, respectively, b, d) measured and fitted ISO and ASHRAE test dust size distributions, respectively.

Table S5: Detailed modal analysis of ISO and ASHRAE test dust samples

Test Dust	Mode #	GM (µm)	GSD (-)	Volume Fraction (%)
ISO Fine	1	0.9	1.2	2.2
	2	4.3	2.5	67.5
	3	32.0	2.0	30.3
ASHRAE #2	1	0.9	1.2	1.9
	2	4.3	2.5	51.0
	3	32.0	2.0	22.9
	4	20.0	1.5	7.0
	5	150.0	2.0	6.1
	6	550.0	1.6	11.0

The size distributions of the recovered dust samples were fitted using the modes introduced in Table S5 with the same GM and GSD but varying volume fractions relative to the test dust. Figures S18a, and S18b, each, illustrate two examples of the measured and fitted size distributions of the recovered dust samples from the ISO- and ASHRAE-loaded MERV 11 filters (i.e., base cases). Error bars on the solid lines represent the minimum and maximum volume distributions from the five LDPS runs of the same sample. The rest of the measured and fitted size distributions of the recovered dust samples in Phase 1 are illustrated in Figures S19 and S20.

The green and red lines in Figure S18 illustrate the cases where we experienced well-fitted and poorly fitted size distributions, respectively. Acquiring a good fit indicates a representative recovery from every single mode although, due to different volume fractions between the recovered and test dust samples, the recovered sample was not necessarily representative (Figure S18: green lines). A poorly fitted case indicates the lack of representativeness not only due to different volume fractions between the recovered and test dust samples but also due to other phenomena such as mode displacement, change in mode GSDs, and/or the appearance of additional modes in the size distribution of the recovered sample. As seen, with the poorly fitted examples, the modes centered on 32 µm in Figure S18a (ISO) and 550 µm in Figure S18b (ASHRAE) the recovered samples have been slightly shifted towards smaller sizes. The displacement of the 550 µm mode in the ASHRAE recovered sample (Figure S18b) could be because of the removal of some larger particles in this mode by the sieve. The displacement could also be explained by the large variations in the amount of the cotton linters from sample to sample or loss of linters during the circulation of the dispersed sample inside the LDPS when it is analyzed for the size distribution. It is often normal to see more variations with larger particles (e.g., > 100 µm) in any sample introduced to the LDPS due to gravitational settling and circulation losses in the LDPS dispersion flow. The shift of the 32 µm mode towards smaller sizes in the samples recovered from ISO-loaded filters and the change in its GM, as seen in the poorly fitted curve in Figure S18a, might be due to the agglomeration of particles in this mode contributing to a larger mode. We found other recovered samples with an appearance of new modes in their size distribution (more examples in Figures S19 and S20). An elevated volume fraction of a new larger mode (as illustrated in Figure S19b) could be evidence of filter fibers being removed and added to the recovered dust during the extraction process, although the volume fraction associated with this new mode was small and negligible.

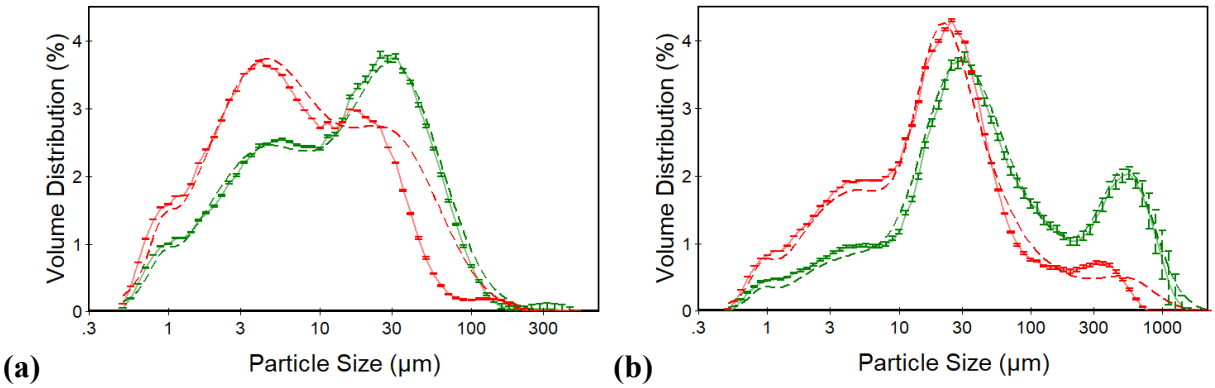

Figure S18: Examples of measured (solid lines) and curve-fitted (dashed lines) size distributions of dust recovered from (a) ISO- and (b) ASHRAE- loaded filters. Green and red lines denote well-fitted and poorly fitted cases, respectively.

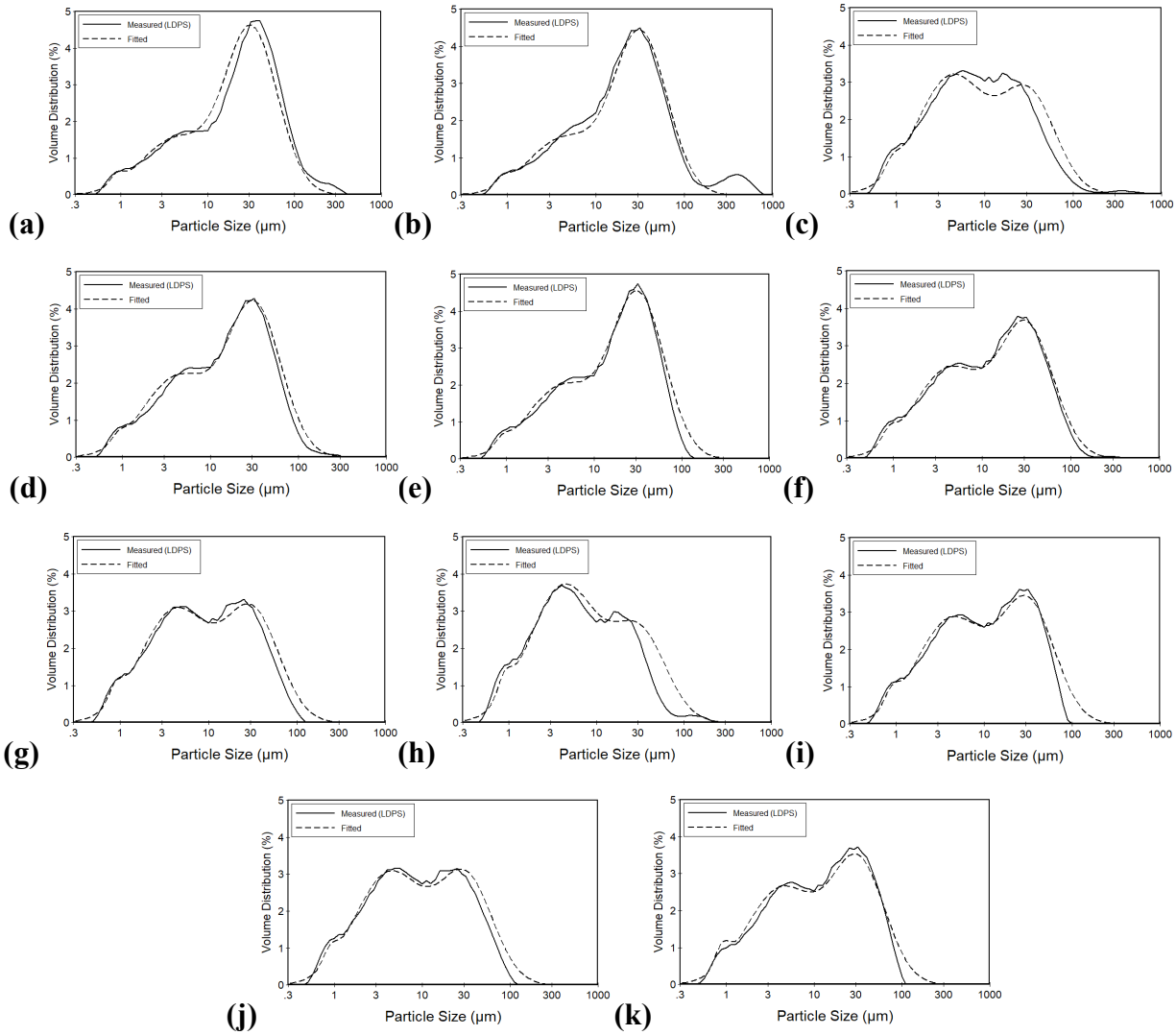

Figure S19: Measured (solid lines) and fitted (dashed lines) size distribution of all the samples recovered from the ISO-loaded filters. a) MERV 8, b,c) MERV 8E d-j) MERV 11 (base case), and k) MERV 14. B and c and d-j are sorted based on the dust mass loaded in filter.

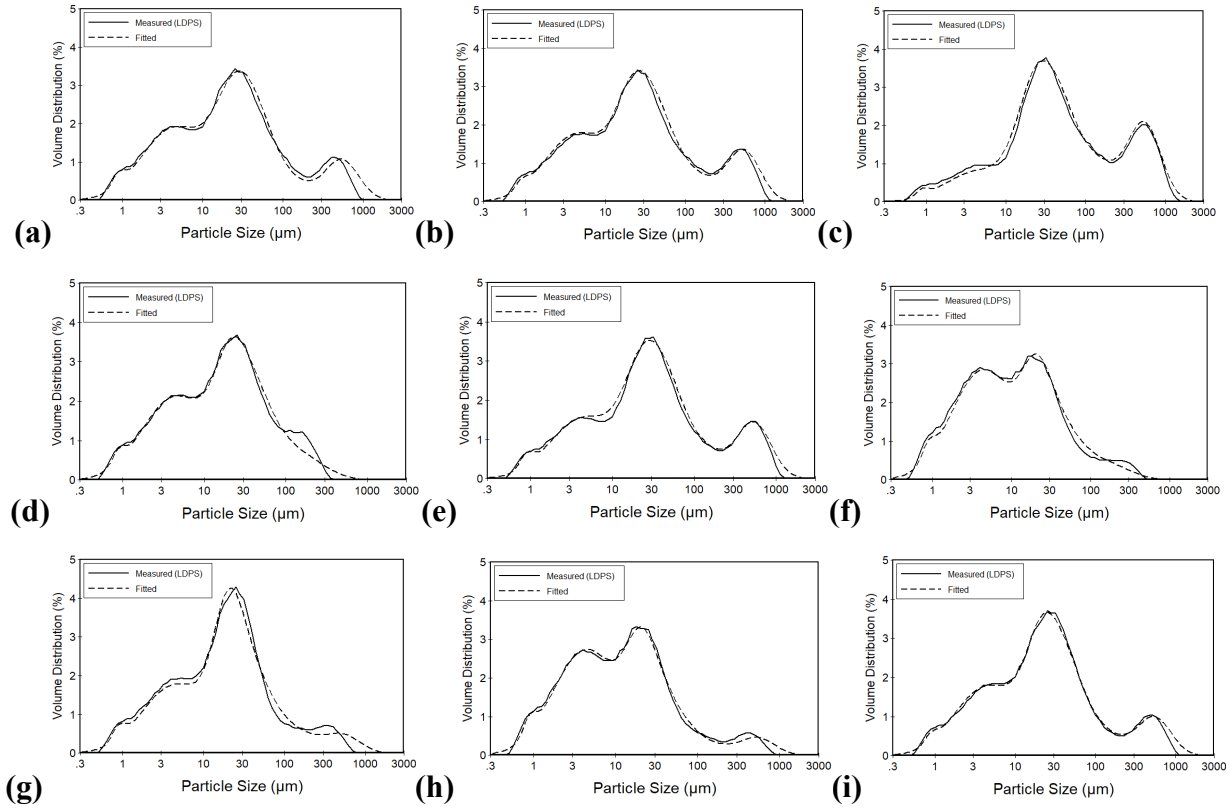

Figure S20: Measured (solid lines) and fitted (dashed lines) size distribution of all the samples recovered from the ASHRAE-loaded filters. a) MERV 8, b) MERV 8E ,c-h) MERV 11 (base case), and i) MERV 14. c-h are sorted based on the dust mass loaded in filter.

Figure S21 illustrates the volume fraction of the modes introduced in Table S5 for all the recovered dust samples. The dashed lines represent the volume fractions of the ISO and ASHRAE test dust samples. As seen, the variations of volume fractions between the cases were often large. The volume fractions of 4.2 and 32 µm modes (modes with highest volume fractions), varied from 30.6 – 66.7% (median = 50.2%) and from 31.4-68.3% (median = 47.7%) among the recovered samples from the ISO-loaded filters (Figure 21a) and from 15.2 – 56.6% (median = 34.9%) and from 24.3 – 48.8% (median = 41.7%) among the recovered samples from the ASHRAE-loaded filters, respectively. The volume fraction of 4.2 µm mode among all the samples from ISO-loaded filters and most of the samples from ASHRAE-loaded filters remained less than that in the ISO and ASHRAE test dust, a further indication of the underrepresentation of this mode in the recovered samples compared to test dust. We observed the volume fractions of the 4.2 µm mode relatively increased with the recovery from the filters that were loaded with more mass of ISO indicating the underrepresentation of this mode in the recovered sample is less of concern if the filter is more heavily loaded (Figure S21a). We also observed large variations in the sum of the volume fractions associated with cotton linters (Modes #4-6 in Table S5) upon extraction from the ASHRAE-loaded filters indicating a large change in the mass of cotton linters from sample to sample and/or loss of the linters to the sieve in the sampler or inside the LDPS.

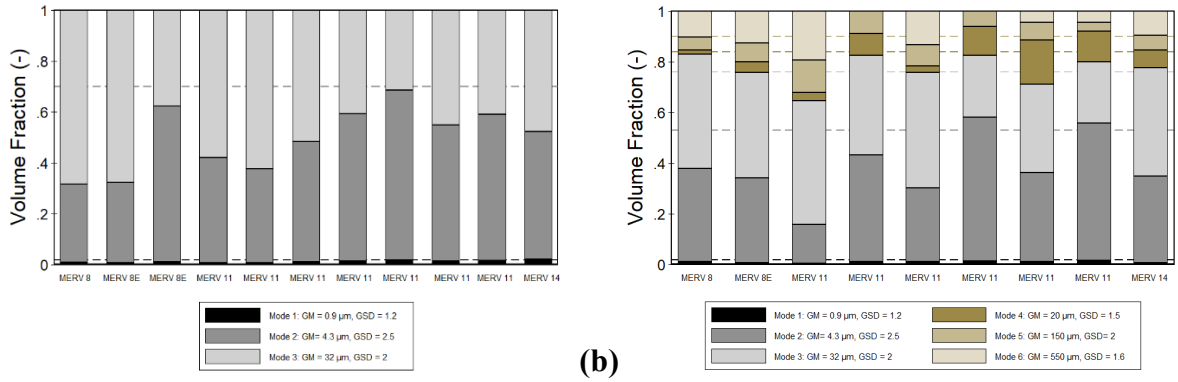

(a) **(b)**

Figure S21: The relative volume fractions of the recovered dust from (a) ISO- and (b) ASHRAE- loaded filters. Dashed lines denote the relative volume fractions of ISO and ASHRAE test dust samples in (a) and (b), respectively.

Phase 2 recovery data: Figure S22 illustrates the box plots of the after-sieve and pre-sieve dust recovery and recovery efficiency samples after the first three extraction cycles in Phase 2 (naturally loaded filters). Figure S23 illustrates the overall, after-sieve, and pre-sieve mass recovery (g) and recovery efficiency (%) for the entire number of cycles performed over the naturally loaded filters. The bullet points connected by a line represent data obtained from a single filter. This figure is another representation of Figure 3 in the main text and Figure S22 (illustrated as box plots) plus the recovery information during extraction cycles #4-6 which is not shown in Figures 3 or S22.

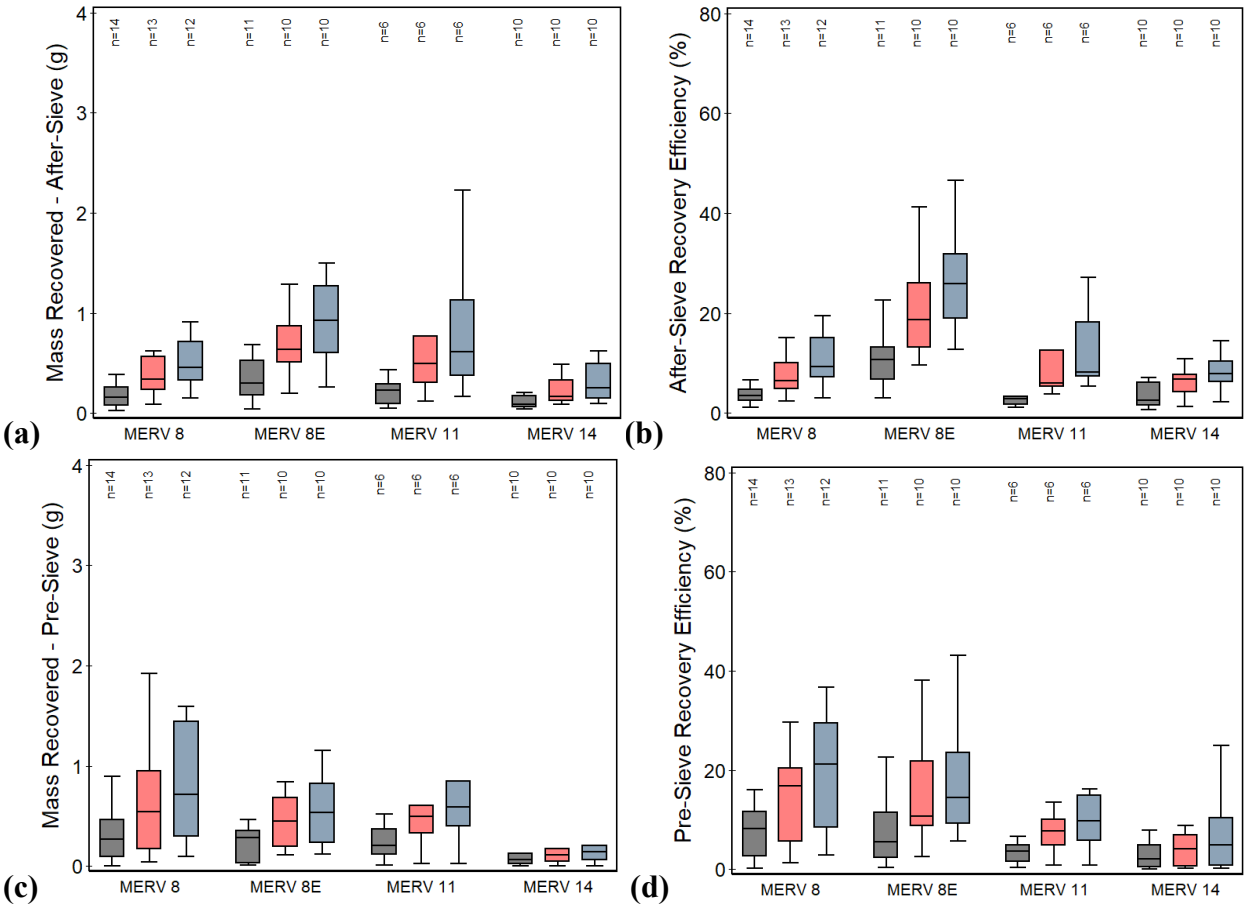

Figure S22: Cumulative pre- and after-sieve mass recovered and recovery efficiency from the naturally loaded filters. Colors denote cycle number (black: cycle 1, red: cycle 2, and blue: cycle 3). n represents the number of filters that are included in each box.

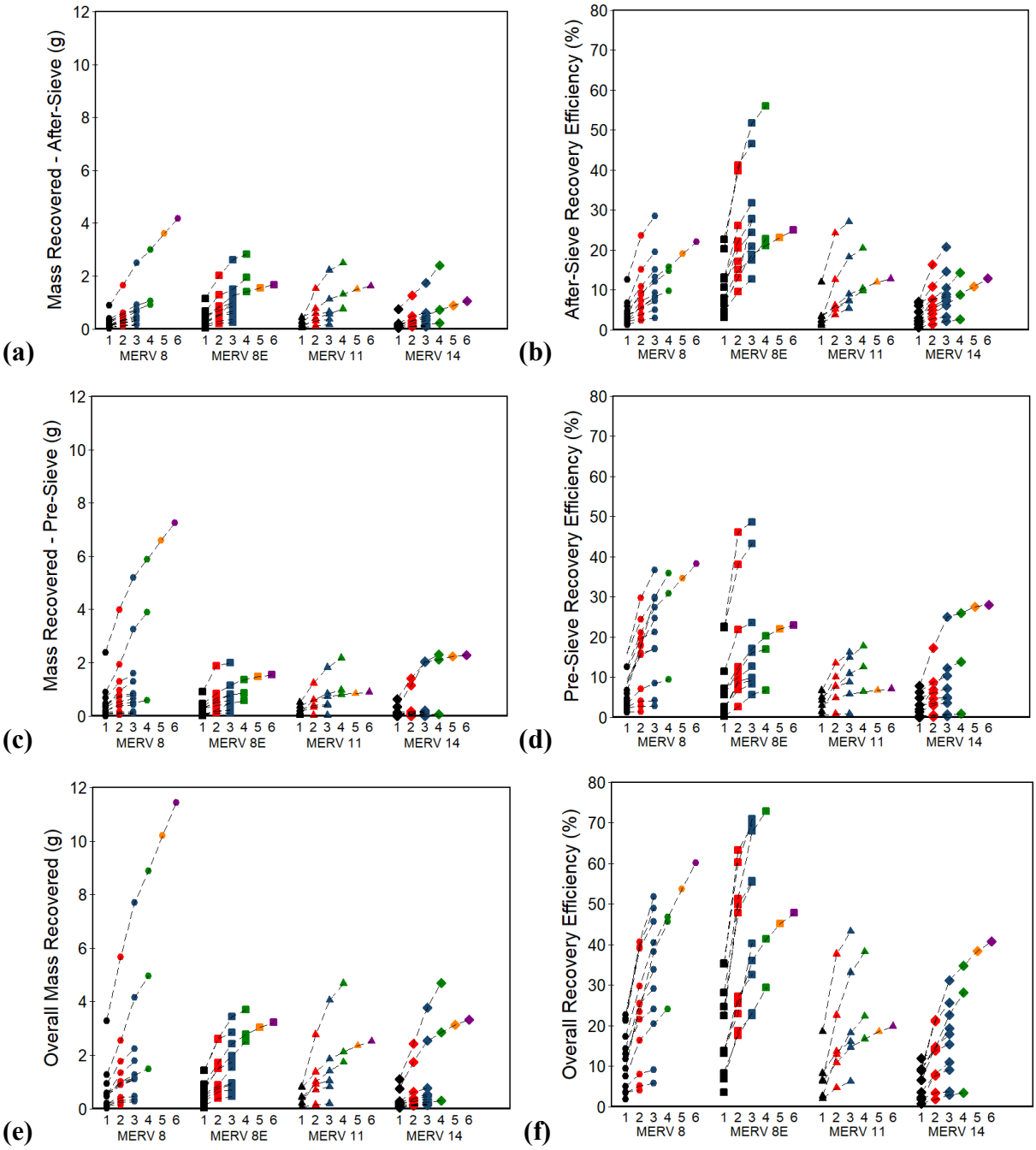

Figure S23: Cumulative pre-sieve, after-sieve, and overall mass recovered and recovery efficiency from the naturally loaded filters. Colors denote cycle number (black: cycle 1, red: cycle 2, and blue: cycle 3, green: cycle 4, orange: cycle 5, and purple: cycle 6).

Concentration and MDL Data

Table S6 summarizes the method detection limit (MDL) and concentration data we obtained from the literature. The MDLs were calculated in µg of analyte enabling the calculations of the

minimum required dust mass in terms of g of dust when combined with the concentration data (µg analyte/g dust). Since the cited references reported their MDLs as µg/(g dust) or µg/(L reagent), we converted their numbers using the basis mass of dust or volume of reagents reported in the same references. With the lack of an MDL reported, the limit of detection (LOD) or limit of quantification (LOQ) (whichever more conservative) was assumed as the MDL. For the semivolatile organic compound (SVOC) groups such as polycyclic aromatic hydrocarbons (PAHs), polybrominated diphenyl ethers (PBDEs), polychlorinated biphenyls (PCBs), and phthalates we calculated the MDL based on the congener from each group that had the highest MDL among all the congeners of the same group. The low and high concentrations summarized in Table S6 are the representatives of typically low and high concentrations of the analytes, respectively, that were selected based on the minimum, 10th, or 25th percentiles and 90th, or 95th percentiles of the ranges reported in the literature for the low and high cases, respectively.

Table S6: MDL and concentration selection from the literature data

Analyte	MDL				Concentration				
	Case	Value (µg)	Reference	Method (1)	Case	Value (µg/g)	Reference	Dust Type (2)	Percentile Selected
Pb	Low	4.8E-4	Kurt-Karakus (2012)	ICP-MS	Low	8.4	Noris et al. (2009)	F	10th
	High	3.0	Al Momani (2007)	ICP-OES	High	357.0	Rasmussen et al. (2013)	S	90th
Cd	Low	8.0E-5	Kurt-Karakus (2012)	ICP-MS	Low	1.0	Noris et al. (2009)	F	10th
	High	0.3	Al Momani (2007)	ICP-OES	High	11.1	Rasmussen et al. (2013)	S	90th
As	Low	0.07	Yang et al. (2015a)	AAS	Low	1.0	Noris et al. (2009)	F	10th
	High	5.3	Siddique et al. (2011)	INAA	High	26.7	Rasmussen et al. (2013)	S	90th
Cr	Low	4.0E-4	Kurt-Karakus (2012)	ICP-MS	Low	58.0	Rasmussen et al. (2013)	S	10th
	High	12.5	Siddique et al. (2011)	INAA	High	177.0			90th
PAHs	Low	0.002	Whitehead et al. (2011)	GC-MS	Low	1.5	Maertens et al. (2008)	S	0th
	High	0.02	Maertens et al. (2008)	GC-MS	High	15.3	Yang et al. (2015b)	S	90th
PBDEs	Low	1.7E-5	Krol et al. (2014)	GC-MS	Low	1.7	Xu et al. (2015)	F	10th
	High	5.9E-4	Chou et al. (2016)	GC-MS	High	30.0			90th
PCBs	Low	6.3E-4	Abb et al. (2010)	GC-MS	Low	0.009	Delavalle et al. (2013)	S	25th
	High	0.004	Kang et al. (2013)	GC-MS	High	0.6			95th
Phthalates	Low	7.5E-4	Kang et al. (2012) (3)	GC-MS	Low	27.0	Xu et al. (2015)	F	10th
	High	0.02		GC-MS	High	3670.0			90th

(1) AAS: Atomic absorption spectrometry, GC: Gas chromatography, ICP: Inductively coupled plasma, INAA: Instrumental neutron activation analysis, MS: Mass spectrometry, OES: optical emission spectrometry

(2) F: Filter dust, S: Settled dust

(3) Low and high MDLS were estimated based on different bases: 0.05 g (low), 1 g (high)

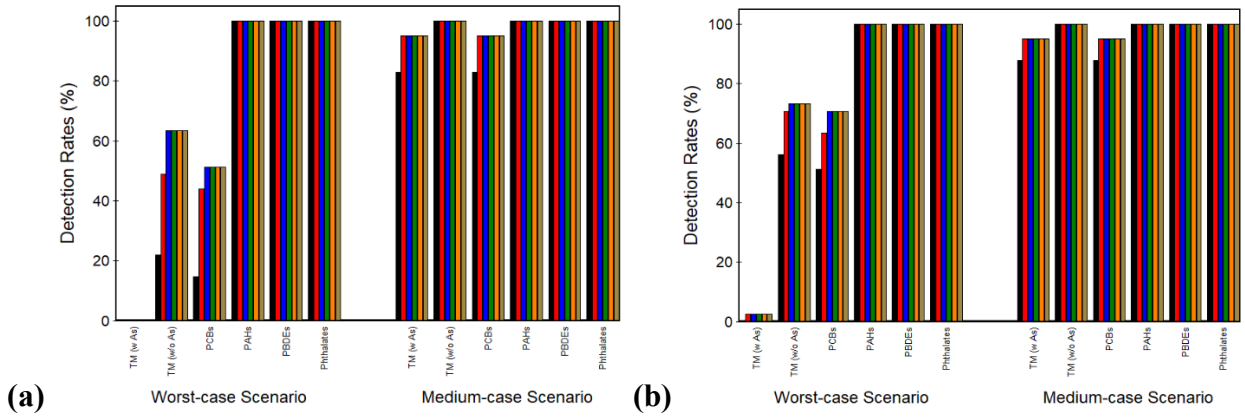

Figure S24: Detection rates of Phase 2 samples in terms of cycle number, analytes, and case scenarios: a) after-sieve dust, b) overall (after-sieve + pre-sieve dust). Colors denote extraction cycles (black, red, blue, green, orange, and brown denote 1-6, respectively)

References

Abb, M., Breuer, J.V., Zeitz, C., Lorenz, W., 2010. Analysis of pesticides and PCBs in waste wood and house dust. Chemosphere 81, 488–493.

Al-Momani, I.F., 2007. Trace elements in street and household dusts in Amman, Jordan. Soil Sediment Contam. 16, 485–496.

Chou, H.-M., Kao, C.-C., Chuang, K.P., Lin, C., Shy, C.-G., Chen, R.-F., Tsai, C.-C., Chuang, C.-Y., Cheng, Y.-C., Chen, C.-C., Chao, H.-R., 2016. Levels of Polybrominated Diphenyl Ethers in Air-Conditioner Filter Dust Used to Assess Health Risks in Clinic and Electronic Plant Employees. Aerosol Air Qual. Res. 16, 184–194.

DellaValle, C.T., Wheeler, D.C., Deziel, N.C., De Roos, A.J., Cerhan, J.R., Cozen, W., Severson, R.K., Flory, A.R., Locke, S.J., Colt, J.S., Hartge, P., Ward, M.H., 2013. Environmental Determinants of Polychlorinated Biphenyl Concentrations in Residential Carpet Dust. Environ. Sci. Technol. 47, 10405–10414.

Haynes (2012) CRC handbook of chemistry and physics. CRC Press; 13 edition.

Kang, Y., Man, Y.B., Cheung, K.C., Wong, M.H., 2012. Risk Assessment of Human Exposure to Bioaccessible Phthalate Esters via Indoor Dust around the Pearl River Delta. Environ. Sci. Technol. 46, 8422–8430.

Kang, Y., Yin, Y., Man, Y., Li, L., Zhang, Q., Zeng, L., Luo, J., Wong, M.H., 2013. Bioaccessibility of polychlorinated biphenyls in workplace dust and its implication for risk assessment. Chemosphere 93, 924–930.

Krol, S., Namiesnik, J., Zabiegala, B., 2014. Occurrence and levels of polybrominated diphenyl ethers (PBDEs) in house dust and hair samples from Northern Poland; an assessment of human exposure. Chemosphere 110, 91–96.

Kurt-Karakus, P.B., 2012. Determination of heavy metals in indoor dust from Istanbul, Turkey: Estimation of the health risk. Environ. Int. 50, 47–55.

Maertens, R.M., Yang, X., Zhu, J., Gagne, R.W., Douglas, G.R., White, P.A., 2008. Mutagenic and carcinogenic hazards of settled house dust I: Polycyclic aromatic hydrocarbon content and excess lifetime cancer risk from preschool exposure. Environ. Sci. Technol. 42, 1747–1753.

Malvern, 1997 Sample dispersion and refractive index guide. MAN0079, version 3.1.
Noris, F., J.A. Siegel, K.A. Kinney. 2009. Biological and Metal Contaminants in HVAC Filter Dust. ASHRAE Transactions. 115, 484–491.
Rasmussen, P.E., Levesque, C., Chenier, M., Gardner, H.D., Jones-Otazo, H., Petrovic, S., 2013. Canadian House Dust Study: Population-based concentrations, loads and loading rates of arsenic, cadmium, chromium, copper, nickel, lead, and zinc inside urban homes. Sci. Total Environ. 443, 520–529.
Seinfeld, J.H., Pandis, S.N., 2016. Atmospheric chemistry and physics: from air pollution to climate change. John Wiley & Sons.
Siddique, N., Majid, A., Tufail, M., 2011. Elemental analysis of dust trapped in air conditioner filters for the assessment of Lahore city's air quality. J. Radioanal. Nucl. Chem. 290, 691–699.
Whitehead, T., Metayer, C., Gunier, R.B., Ward, M.H., Nishioka, M.G., Buffler, P., Rappaport, S.M., 2011. Determinants of polycyclic aromatic hydrocarbon levels in house dust. J. Expo. Sci. Environ. Epidemiol. 21, 123–132.
Xu, Y., Liang, Y., Urquidi, J.R., Siegel, J.A., 2015. Semi-volatile organic compounds in heating, ventilation, and air-conditioning filter dust in retail stores. Indoor Air 25, 79–92.
Yang, Q., Chen, H., Li, B., 2015a. Source Identification and Health Risk Assessment of Metals in Indoor Dust in the Vicinity of Phosphorus Mining, Guizhou Province, China. Arch. Environ. Contam. Toxicol. 68, 20–30.
Yang, Z.-Z., Li, Y.-F., Fan, J., 2015b. Polycyclic aromatic hydrocarbons in deposited bedroom dust collected from Xinxiang, a fast developing city in North China. Environ. Monit. Assess. 187.